A NUMERICAL COMPARISON OF LIFT PERFORMANCE OF TWO DIFFERENT AIRFOILS USED FOR DOMESTIC WIND TURBINE

Esam Hamza*, Seraj Fathi*, Mohamed M. Albarghot, Ismaeel M. Belal** and Basim Freegah*****

*Department of Mechanical and Industrial Engineering, Faculty of Engineering, University of Tripoli, Tripoli, Libya
** Department of Energy Storage, The Libyan Center for Solar Energy Research, and studies, Tajoura-Tripoli-Libya
***Mechanical Engineering Department, Engineering College, Al-Mustansiriya University, Baghdad-Iraq
Email: es.hamza@uot.edu.ly
Received 20 May 2025, revised 24 May 2025, accepted 26 May 2025

الملخص

في ضوء الطلب العالمي المتزايد على الطاقة، تستكشف هذه الدراسة إمكانات توربينات الرياح الصغيرة الحجم لتوليد الطاقة محليًا أو منزليا. بالتركيز على زعانف التربينات الهوائية، والتي تعتبر المكونات الأساسية لشفرات توربينات الرياح، تبحث الدراسة الحالية في أداء تصميمين مختلفين وهما NREL S826 وNACA 2412 . لتحقيق ذلك، تم بناء نموذج عددي ثنائي الأبعاد لكل نوع من الزعانف الهوائية. استخدمت النماذج العددية مجالًا حسابيا من النوع C وتضمنت توليد شبكة حسابية مع استخدام تقنية التضخيم بالقرب من الحدود للحصول على تمثيل دقيق. تم أيضاً استخدام نموذج الاضطراب Spalart-Allmaras لتحليل الديناميكيات المعقدة لتدفق المائع حول الزعانف الهوائية ولضمان موثوقية النموذج العددي المطور تمت مقارنة النتائج ببيانات معملية معتمدة. يتضمن البحث الحالي فحصًا معمقًا لتوزيعات الضغط والسرعة حول الزعانف عند سرعات رياح مختلفة (5.5 م/ث، 7 م/ث، 8.3 م/ث، و 9.7 م/ث) وزوايا هجوم (0°، 2°، 4°، 6°، 8°، 10°، 12°، 14°، و 16°). أحد الجوانب المهمة لهذه الدراسة يتضمن مقارنة معامل الرفع وقوة الرفع التي تولدها كل زعنفة في ظل ظروف التشغيل المتنوعة التي تم أخذها في الاعتبار. كشفت النتائج أنه بالنسبة لزاويا الهجوم التي تتراوح من 12 درجة إلى 14 درجة، حققت كلا الزعنفتين أداء الرفع الأمثل. ومن المثير للاهتمام، أن الزعنفة الهوائية NREL S826 أظهرت أفضلية وبشكل طفيف ضمن هذا النطاق الأمثل. عند أعلى سرعة رياح (9.7 م/ث)، حققت الزعنفة NREL S826 أقصى معامل رفع يبلغ 4.9176 عند زاوية هجوم 14 درجة، متجاوزًا الحد الأقصى لـ NACA 2412 البالغ 3.6878 عند 12 درجة بنفس سرعة الرياح.

ABSTRACT

In light of the increasing global demand for energy, this study explores the potential of small scale (domestic) wind turbines for generating energy domestically. Focusing on airfoils, which are the main elements of wind turbine blades, the research examines the performance of two different designs: NREL S826 and NACA 2412. For this purpose, two-dimensional numerical model was created for each airfoil. The models utilised a C-type grid and incorporated mesh generation with boundary inflation for accurate representation. The Spalart–Allmaras turbulence model was employed to examine the intricate dynamics of flow surrounding the airfoils and to guarantee the precision of the developed numerical model, the outcomes were contrasted with verified experimental data. The current research involved an in-depth examination of pressure and velocity distributions over the airfoils at different wind speeds (5.5 m/s, 7 m/s, 8.3 m/s, and 9.7 m/s) and angles of attack (0°, 2°, 4°, 6°, 8°, 10°, 12°, 14°, and 16°). One of the critical aspects of this study encompasses comparing the lift coefficient and the lift force generated by each airfoil under the diverse operating conditions that were considered. The findings revealed that for the angle of attack ranging from12° to 14°, both airfoils achieved their optimal lift performance. Interestingly, the NREL S826 airfoil demonstrated a slight preference within this optimal range. At the highest wind speed (9.7 m/s), the NREL S826 achieved a maximum lift coefficient of 4.9176 at an angle of attack of 14°, exceeding the NACA 2412's maximum of 3.6878 at 12° at the same wind speed.

KEYWORDS: Airfoils, Domestic Wind Turbine, Computational Fluid Dynamics (CFD), Spalart-Allmaras turbulence model, Lift Coefficient.

INTRODUCTION

Due to rising population and consumerism, the world's energy demand is growing virtually everyday, causing environmental damage and an energy crisis. Fossil fuel-derived energy is still unsustainable because of its finite supply, depletion, and environmental effects. Thus, there is a greater need for sustainable, eco-friendly, and alternative energy sources [1]. The transition to renewable energy, which produces zero carbon emissions when used, helps address not only climate change but also air pollution, global health, and the economy. Renewable energy comes from sources like the sun and wind, which naturally regenerate and provide an endless supply of power. Renewable energy serves various purposes, including generating electricity, heating and cooling spaces and water, and powering transportation. Wind energy has seen remarkable progress in technology, efficiency, and cost reduction in recent years. The declining cost of wind-generated electricity has made it a highly competitive option among energy sources [2]. Interestingly, renewable energy like wind, Solar, and hydro energy are expanding rapidly and are expected to play a vital role in meeting future needs without reliance on fossil fuels—particularly wind energy, which holds substantial potential. Evidently, wind power is becoming more cost-competitive with traditional energy sources, and technological advancements are enhancing its efficiency. Wind farms are emerging worldwide, capturing wind energy to produce clean electricity. This not only cuts greenhouse gas emissions but also strengthens energy diversity, making it more resilient and less vulnerable to fluctuations in fossil fuel prices. With ongoing innovation and investment, wind energy is set to play a crucial role in shaping the future of the global energy sector [3]. In Figure 1, The transformation of the global energy supply is presented where it graphs global energy consumption from 1800 onwards [4].

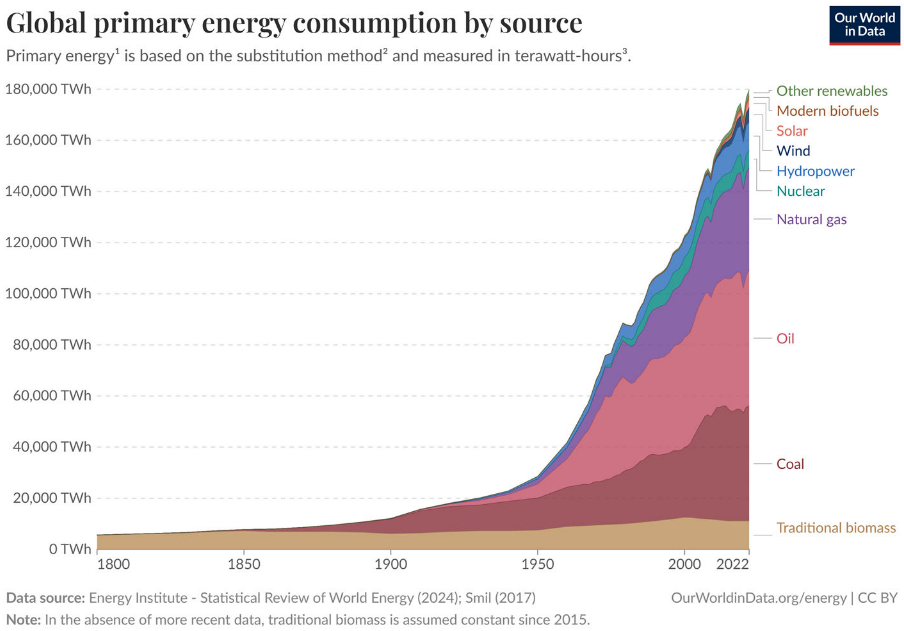

Figure 1: The transformation of the global energy supply [4].

Wind power or wind energy, a renewable power source, captures the force of the wind to produce electricity. Wind turbines play a key role in this process by converting the rotational movement of their blades—driven by kinetic energy from moving air into electrical energy. This transformation relies on specific technologies, including a generator positioned at the top of a tower within the nacelle. Wind turbines, whether large or small, generate electricity for utilities, homeowners, and remote villages. This renewable energy source paves the way for a more sustainable and prosperous future, benefiting both humanity and all living creatures. Additionally, wind energy proved particularly valuable in regions with limited sunlight, such as high-latitude countries where solar energy production may be less effective [5,6]. Wind energy contributes 5% of global electricity generation and 8% of the U.S. power supply. In 2022, an additional 77.6 GW of wind capacity was integrated into global grids, marking a 9% growth compared to 2021. That year, the total installed wind energy capacity worldwide soared to 900 GW enough to power millions of homes. Onshore and offshore wind capacity now exceeds 743 gigawatts, surpassing grid-connected solar energy and amounting to roughly half of hydropower's output. Notably, nearly three-quarters of the 651 gigawatts of installed wind capacity originate from wind farms in China, the U.S., Germany, India, and Spain. Moreover, both onshore and offshore wind energy continue to hold immense potential for expansion and technological advancement on a global scale [7-10].

Small-scale wind turbines are primarily used in homes, and small commercial purposes to generate electricity. These turbines come in various power ratings, typically below 50 kilowatts. The higher a turbine's rated power, the greater the wind speed required to rotate its blades efficiently and achieve maximum output. Each turbine has a specific cut-in speed, the minimum wind velocity needed to start generating electricity. Small-scale wind turbines be installed on-grid or off-grid, providing localized power and often part of hybrid systems with solar panels and battery storage. Moreover, it has shorter towers, optimized for local wind conditions. Selecting the right turbine should be based on available wind data, as choosing an unsuitable model can affect performance. Additionally, improper placement of wind turbines is a common mistake that can significantly impact their efficiency [11]. Wind energy harvesting involves transforming the kinetic energy of moving air into electricity using wind turbines. Several factors influence the efficiency of energy capture, with wind speed being a key element. Turbines require a minimum wind speed of 14.5 km/h to begin rotating and generating power, while optimal energy production occurs at speeds ranging between 40 and 56 km/h [12]. The length of a wind turbine's blades directly impacts the amount of energy it can capture. Longer blades enhance energy collection from the wind, but they also necessitate more robust support structures to maintain stability [13]. Blade pitch, or the angle at which the blades are positioned in relation to the wind, influences the amount of energy they can capture. Additionally, the efficiency of the generator determines how efficiently mechanical energy is converted into electrical power [14].

Computational Fluid Dynamics (CFD) as a Method for Airfoils performance Analysis.

This approach numerically solves the fundamental equations governing fluid dynamics. The continuous domain is segmented into small volumes, forming a mesh or grid, where complex partial differential equations are solved. With advancements in computational power, the use of (CFD) for studying and analysing wind turbines has become increasingly prevalent. By implementing appropriate models and hypotheses, CFD simulations can serve as a valuable tool for testing and qualitatively comparing various configurations and operating conditions. This approach helps identify the most promising designs before advancing to prototype construction and experimental testing [15-18].

John E. Matsson et al [19], conducted a study on the NACA 2412 airfoil, focusing on its design, testing, and analysis. They used a multi-manometer to measure the lift coefficient at different angles and verified their results through CFD analysis in Ansys, which closely aligned with experimental data.

A study was presented by M. Tech Scholar [20] to examine inviscid flow over the NACA 4412 airfoil, focusing on lift and drag characteristics to minimize dependence on wind tunnel testing. Utilizing ANSYS FLUENT, researchers analysed surface pressure distribution and computed drag and lift using integral equations. The findings closely aligned with experimental results, confirming CFD as a dependable method for aerodynamic assessment.

Ronit K. Singha and M. Rafi Uddin Ahmed [21], developed the AF300 airfoil for small horizontal axis wind turbines, aiming to enhance start up and low wind speed performance. They evaluated its aerodynamics through experimentation, CFD analysis, and PIV studies. Their findings showed lift-to-drag ratios and lift coefficients, identifying a stall at a 14° angle of attack (AOA). For Reynolds numbers ranging from 75,000 to 205,000, the maximum lift coefficient (CLmax) reached 1.72, 1.81, and 1.86, demonstrating the airfoil's efficiency in low Reynolds number conditions.

Abdulkadir Ali and Harun Chowdhury [22], analysed the aerodynamic characteristics of a small Horizontal Axis Wind Turbine (HAWT) with three different blade designs: upwind winglet, downwind winglet, and a straight blade without a winglet. Utilizing the SG6051 airfoil, specifically designed for small wind turbines, they conducted wind tunnel experiments at RMIT to measure aerodynamic forces. Their results revealed that the upwind winglet increased the lift-to-drag ratio by 26%, while the downwind winglet decreased it by 27%.

Thin Dinh Vana and Duc Nguyen Huu [23], conducted an optimization study on blade configurations using the SG6043 airfoil model, evaluating ten different lengths from 1 m to 10 m to identify the most suitable design for a rated wind speed of 5 m/s in Vietnam. They applied the Betz optimization method in Qblade software to refine chord and twist values. Key aerodynamic characteristics, such as lift coefficient (Cl), drag coefficient (Cd), power factor (Cp), and power (P), were assessed using XFLR5 and Qblade. Additionally, operational parameters like pitch angle and rotor speed were examined to enhance wind energy efficiency. Their findings revealed a peak Cp of 0.476 and a maximum power output of 95.319 kW within a wind speed range of 1 m/s to 5 m/s.

Y.F. Gorgulu et al. [24], conducted a study on the aerodynamic behaviour of the NACA 0009 airfoil at a constant Reynolds number using CFD. They examined lift coefficient, drag coefficient, and lift-to-drag ratios across angles of attack ranging from 0° to 15° in 5° steps. Wind tunnel experiments were performed with a free airflow velocity of 5 m/s. The results indicated that assessing lift and drag forces independently provided the most accurate findings at two specific angles, with the best aerodynamic performance occurring at a 5° angle of attack.

M . Islam et al. [25] carried out an investigation on laminar separation bubbles (LSBs) over the SD 7003 airfoil at low Reynolds numbers using OpenFOAM and a laminar kinetic energy-based transition model. They examined two versions of the k-kL-ω transition model, derived from Pohlhausen and Falkner-Skan profiles, to evaluate pressure-gradient effects on natural transition. Both variants underestimated lift coefficients while slightly overestimating drag coefficients. Although both models improved predictions of laminar boundary layer separation, they caused significant delays in reattachment. The Falkner-Skan variant demonstrated a more precise reattachment location, showing better agreement with experimental and computational data.

A research conducted by E. Mollica and A. Timmoneri [26], on the low Reynolds S1223 airfoil, modelling its performance and evaluating it numerically using the OpenFOAM. The numerical results were validated against experimental data. A key aspect of their research was a sensitivity analysis of the airfoil's aerodynamic performance across a wide range of Reynolds numbers, specifically Re = 2e04, Re = 2e05, and Re = 2e06. The findings indicate that the curve slope remains largely unaffected by the Reynolds number. However, as the Reynolds number increases, the lift curve shifts upward, and the angle of attack at which maximum lift occurs also increases.

Although airfoil operation is relatively simple, accurately predicting its aerodynamic and mechanical behaviour remains challenging, especially in fluctuating wind conditions. A major concern for wind turbines is performance degradation, making it essential to understand wind dynamics as many nations pursue ambitious wind energy initiatives. This study examines airflow at varying wind speeds and inclinations around the airfoil, utilizing a two-dimensional numerical model for two airfoil types used in small-scale wind turbines. Additionally, the performance characteristics of these airfoils under different conditions are evaluated.

METHODOLOGY

To accomplish the previously established research objectives, the airflow around the airfoil has been simulated numerically using Computational Fluid Dynamics (CFD) techniques. The following flowchart, Figure 2 outlines the methodology used to validate the model.

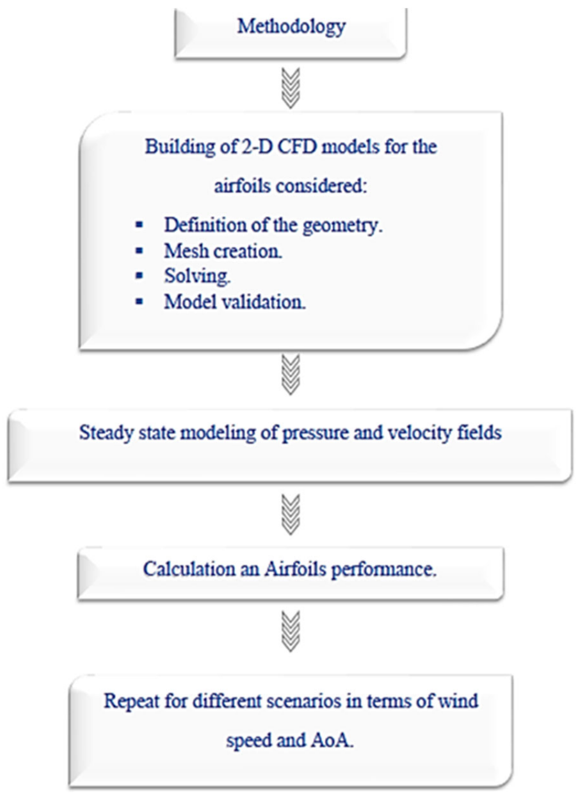

Figure 2: The current research work methodology.

Numerical Modelling

This section details the development of numerical models for the S826 and 2412 airfoils, designed by the National Renewable Energy Laboratory (NREL) and the National Advisory Committee for Aeronautics (NACA), respectively. These airfoils are utilized in the urban environment of Yefran, where wind conditions frequently fluctuate in magnitude and direction. Their innovative design enhances lift generation relative to drag, enabling efficient torque production at low wind speeds and ensuring a reliable startup.

Model description

CFD analysis serves as a virtual testing platform for the NREL S826 and NACA 2412 airfoils, widely used in domestic wind turbines. This method simulates airflow around the airfoil shapes, enabling predictions of aerodynamic performance in terms of lift, drag, and power generation. Engineers can modify wind speeds and assess the airfoil's behavior, refining its design to adapt to the fluctuating wind conditions found in residential settings. This analysis is essential for optimizing energy capture at low wind speeds, a crucial factor for household wind power applications. Figures 3 and 4 illustrate the specific geometries of the NREL S826 and NACA 2412 airfoils.

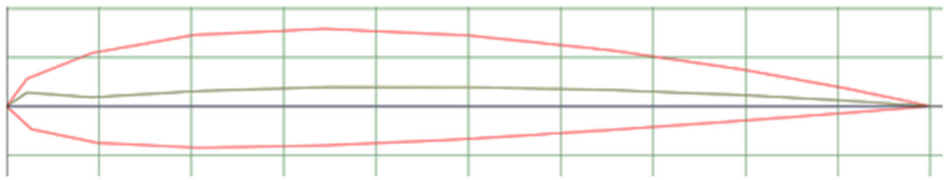

Figure 3: NACA 2412 airfoil [27].

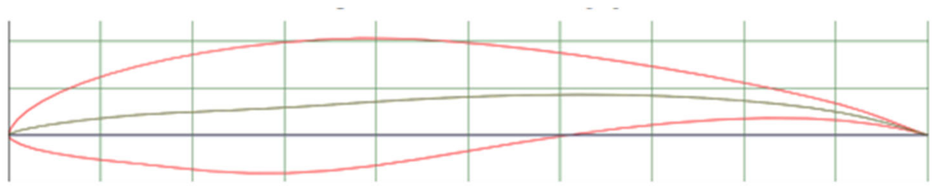

Figure 4: NREL s826 airfoil [27].

Numerical modelling approach

The predicted flow field and airfoils performance data presented in this work have been obtained from numerical analysis using a commercial Computational Fluid Dynamics (CFD) code ANSYS Fluent [28]. This section provides a detailed description of the modeling approach used in which model design, grid generation, boundary conditions and numerical formulation.

Computational hardware

Numerical analysis was conducted on multiple parallel workstations utilizing an Octa-core AMD Ryzen 9 7940HS processor with Radeon 780M, operating at a clock speed of 4.00 GHz and supported by 16GB of PC2933MHz DDR4 memory. The analysis was performed on a high-performance laptop, which executed parallel batch computations, allocating up to eight processing cores per analysis based on the discretized size of the computational domain. A typical analytical run under single-variable and constant conditions took approximately 12–16 minutes to complete using this device.

Design modeler

The numerical model of the airfoils used in this study was designed using the ANSYS program (Design Modeler) workspace. The coordinates of the airfoils were taken from the source that created them and were included in the workspace and its processors to be suitable for conducting analyzes. Table (1) includes the main characteristics of these airfoils.

Table 1: The main characteristics of the considered airfoils.

NACA 2412	NREL s826
1 meter chord length.	1 meter chord length.
Maximum camber of 2% of the chord length.	Maximum thickness is 14% of the chord length.
Location of maximum camber at 40% of the chord length from the leading edge.	Location of maximum at thickness at 33.7% of the chord length from the leading edge.
Thickness of 12% of the chord length.	
The airfoil coordinates were plotted using 200 points for accuracy.	The airfoil coordinates were plotted using 200 points for accuracy.

A C-domain was drawn in the XY plane to represent the Fluid medium (air) and determine the size of the analysis. The entrances, exits and walls were defined for simulating wind tunnel. The C-domain of control is one of the preferences of the forms used in the analysis of airfoils. The dimensions of the domain for the airfoil NACA 2412 are 15m width and 9m radius of arc, while the area of fluid domain is 397.15m² which is splinted to four faces. Regarding the airfoil NREL s826, the dimensions of domain are 15m width and 7.5m radius of arc, while the area of fluid domain is 313.27m² which is also splinted to four faces. Figures 5 and 6 show the domains for both considered airfoils.

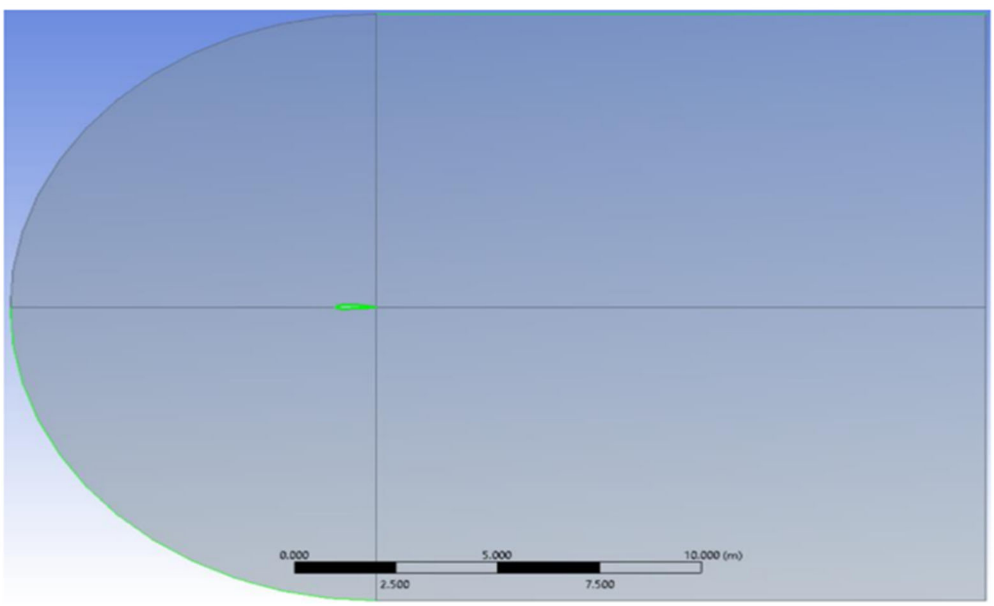

Figure 5: NACA 2412 computational domain.

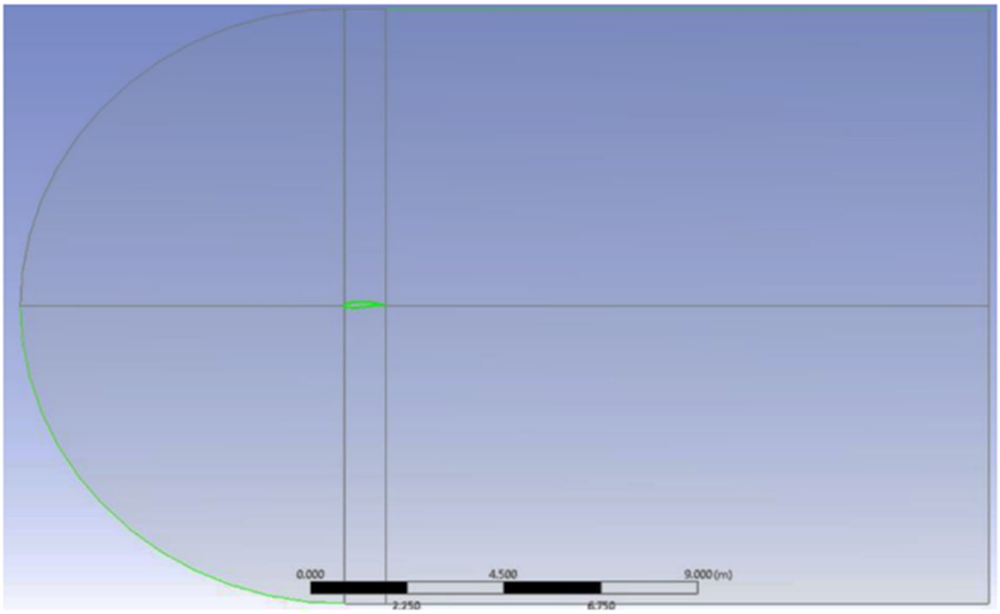

Figure 6: NREL s826 computational domain.

Mesh generation

In order to discretize the computational domain, a C-type grid has been utilised and incorporated mesh generation with boundary inflation for accurate representation**.** To catch the behaviour of flow around the airfoils, the domain has also been projected in to four parts where both structural and unstructured meshing were used. Figures 7and 8 show the mesh dimension that was used in analyzing the airfoils:

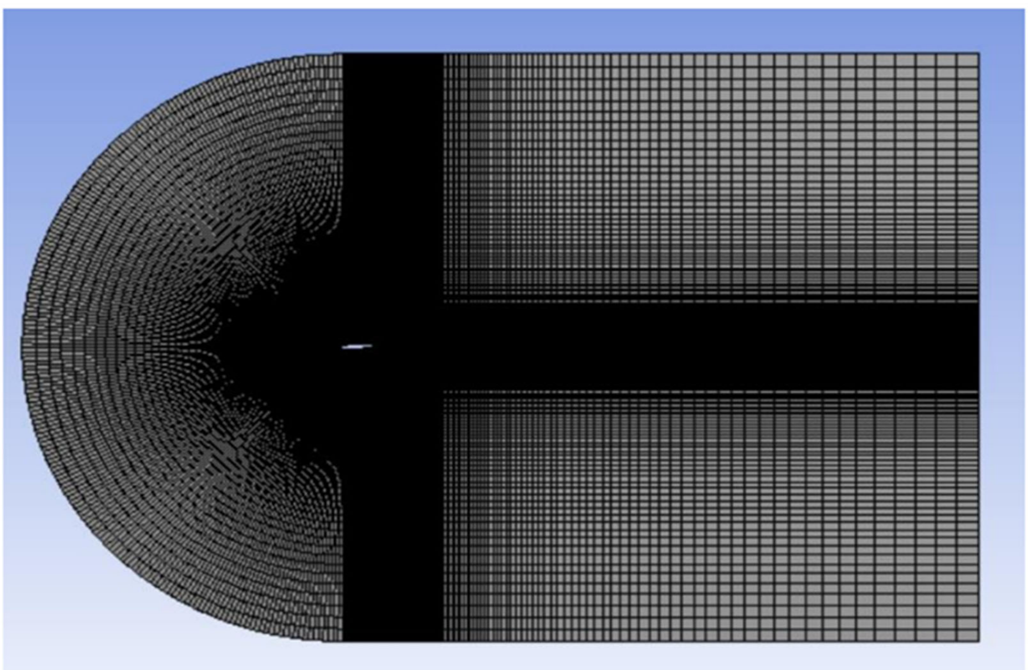

Figure 7: 2D view of NACA 2412 mesh in XY plane.

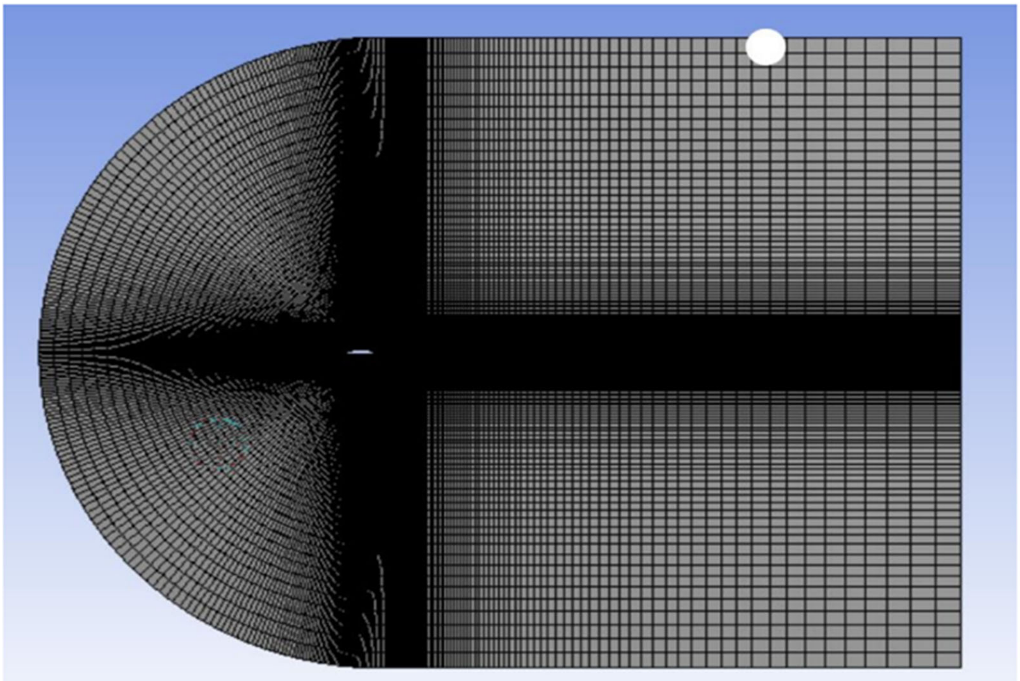

Figure 8: 2D view of NREL s826 mesh in XY plane.

Mesh independence test

To confirm mesh independence, five different grids were analysed under identical solver and flow conditions in the CFD model. The details of the control volumes (elements) used are provided in Tables (2) and (3). The lift coefficient of the airfoil exhibits only minor variation across the grids, with a maximum deviation of 3.30%, which does not warrant the additional computational resources required for larger grids.

Table 2: Mesh independence test for NACA 2412.

NACA 2412					
No. of Elements	8000	12000	50000	128000	200000
AOA	CL	CL	CL	CL	CL
10°	1.35E+00	1.36E+00	1.36E+00	1.36E+00	1.36E+00
12°	1.36E+00	1.37E+00	1.39E+00	1.39E+00	1.39E+00
14°	1.29E+00	1.30E+00	1.33E+00	1.35E+00	1.35E+00
16°	1.20E+00	1.22E+00	1.25E+00	1.28E+00	1.28E+00

Table 3: Mesh independence test for NREL s826.

NREL s826					
No. of Elements	7000	17000	67000	112000	194000
AOA	CL	CL	CL	CL	CL
10°	2.94E+00	3.15E+00	3.43E+00	3.44E+00	3.44E+00
12°	3.40E+00	3.65E+00	3.69E+00	3.69E+00	3.69E+00
14°	3.37E+00	3.65E+00	3.67E+00	3.67E+00	3.67E+00
16°	2.80E+00	3.08E+00	3.15E+00	3.15E+00	3.15E+00

Study boundary conditions and wind properties

The range of wind speeds in Yefran region - Libya was collected and measured at an altitude of 698 meters above sea level. The specific boundary conditions for the study are specified as follows: inlet velocities are 5.5, 7, 8.3, and 9.7 m/s. Angles of attacks are 0, 2, 4, 6, 8, 10, 12, 14, 16, and 18 degrees. The air properties at the specified location: density is 1.18kg/m^3, and viscosity is 1.84e-05 kg/m-s.

Spalart-Allmaras turbulent model

The Spalart-Allmaras turbulence model is a single-equation turbulence model tailored for computational fluid dynamics (CFD) simulations, enabling the prediction of turbulent flow behavior, especially in aerodynamic applications such as airfoil and aircraft performance analysis. Unlike other turbulence models, it utilizes a single transport equation for modified turbulent viscosity, enhancing computational efficiency while maintaining accurate predictions for external flow scenarios [29].

Validation

The numerical model has been validated against the experimental results for the lift coefficient output of NACA 2412 and NREL s826 airfoil [29,30] as shown in Figures 9 and 10. The charts show that S-A model gives results closest to experiments results, with an error rate ranging between 1% and 12%. Therefore, the developed model was used to conduct the investigation in the current study [31-33].

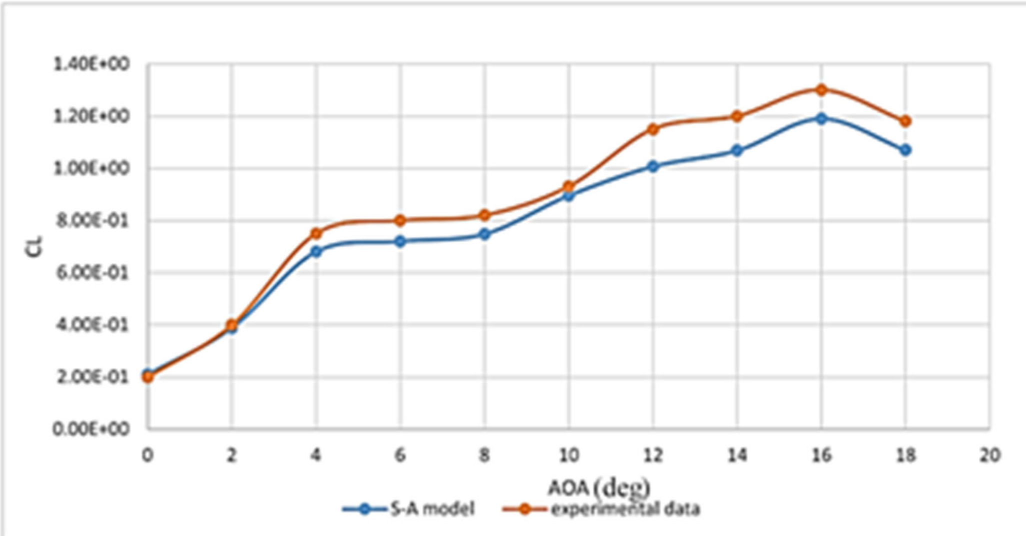

Figure 9: Validation of NACA2412 model using experimental data.

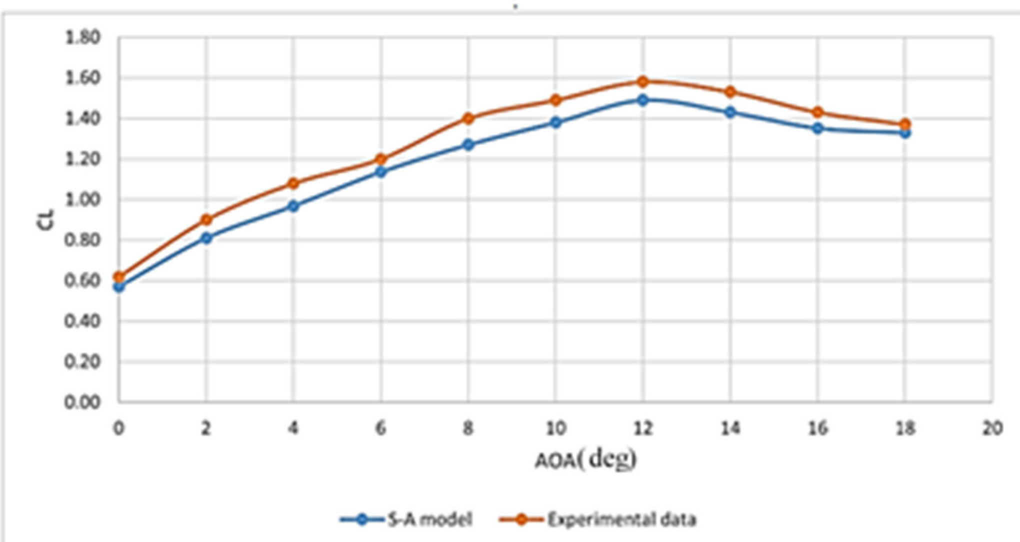

Figure 10: Validation of NREL s826 model using experimental data.

RESULTS AND DISCUSSIONS

The current work primarily examines the flow field characteristics of two airfoils using numerical methods. It quantifies the variations in pressure and velocity as functions of inlet air velocity magnitude and direction over 2D models, ensuring a comprehensive understanding of the flow field. Additionally, these effects are analyzed through the lift coefficient and lift force generated by the airfoils. Velocity and pressure diagrams are employed to visualize airflow distribution and gradients, illustrating how changes in velocity and angle of attack influence the aerodynamic performance of the airfoils.

Velocity Distribution

As can be seen in Figure 11 (a, b, c, d, e, f, g, h) and Figure 12 (a, b, c, d, e, f, g, h) how velocity field around the airfoils are influenced according to the change in the values of AOA at two different wind speed which are 5.5m/s and 9.7m/s. The velocity contours illustrate a notable decrease in speed, nearing zero at the stagnation point on the leading edge due to the abrupt interaction with the airfoil. As the flow approaches the boundary layer, velocity gradually diminishes until it reaches zero at the airfoil surface, a consequence of the no-slip condition in fluid mechanics, where a viscous fluid adopts the velocity of the solid surface it contacts. This low-velocity zone appears in blue within the contour plot. The velocity disparity between the upper and lower airfoil surfaces primarily stems from its shape and the angle of attack in relation to the incoming airflow, governed by two fundamental principles. It is worth mentioning that airfoils are typically not flat; they feature a curved upper surface known as camber and are positioned at an angle to the incoming airflow which is the angle of attack. Accordingly, the curved upper surface of the airfoil causes the airflow to cover a greater distance than the flatter lower surface within the same time frame to reach the trailing edge. As a result, the airspeed above the upper surface increases, in accordance with Bernoulli's principle. Moreover, When the airfoil is positioned at an angle to the airflow, it redirects the air upward over the curved upper surface, enhancing the velocity disparity between the upper and lower surfaces. This effect intensifies as the angle of attack increases, reaching a critical stall point at 12 degrees.

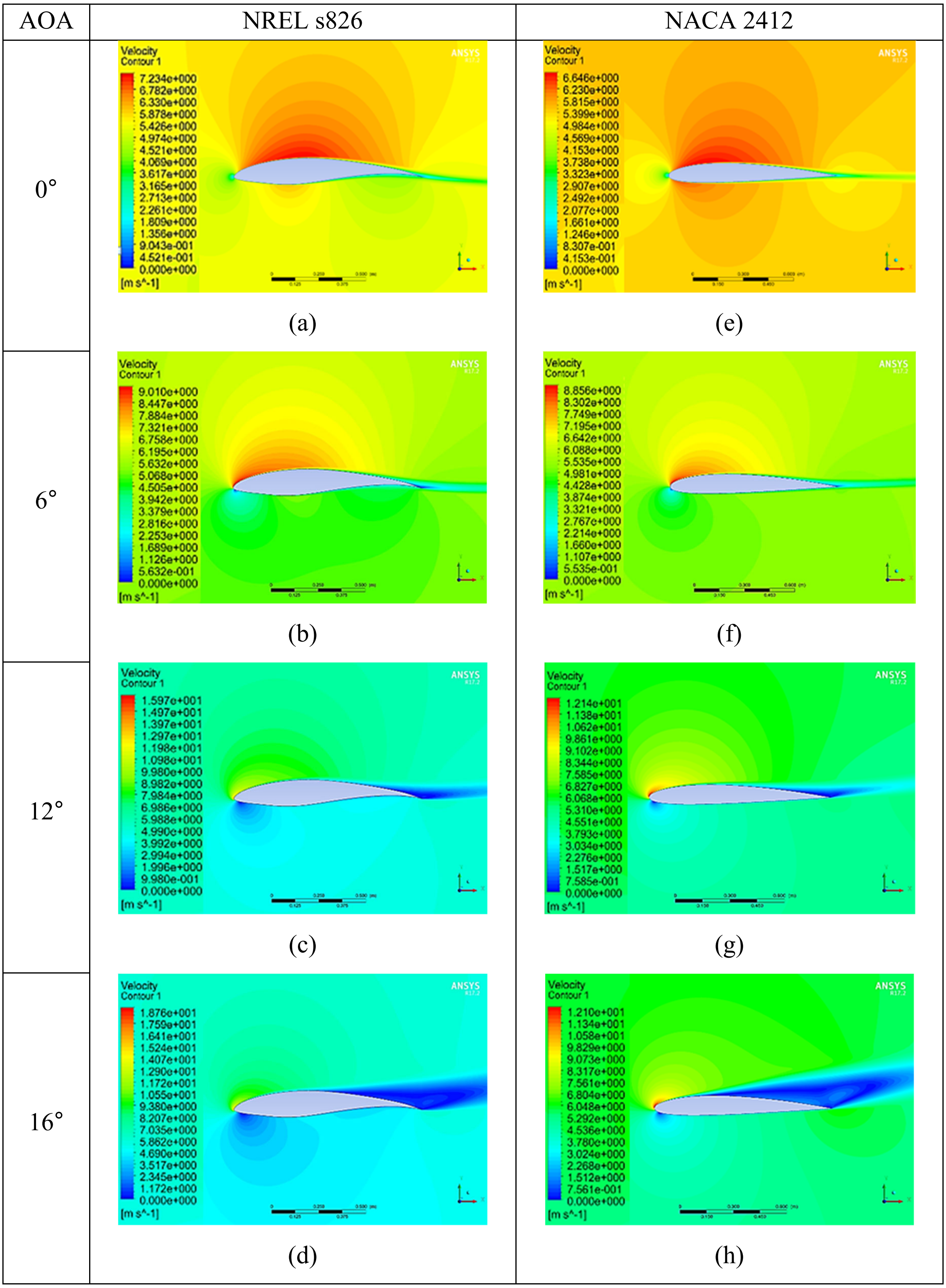

Figure 11: Velocity fields (contours) of airfoils at 5.5m/s for different AOA.

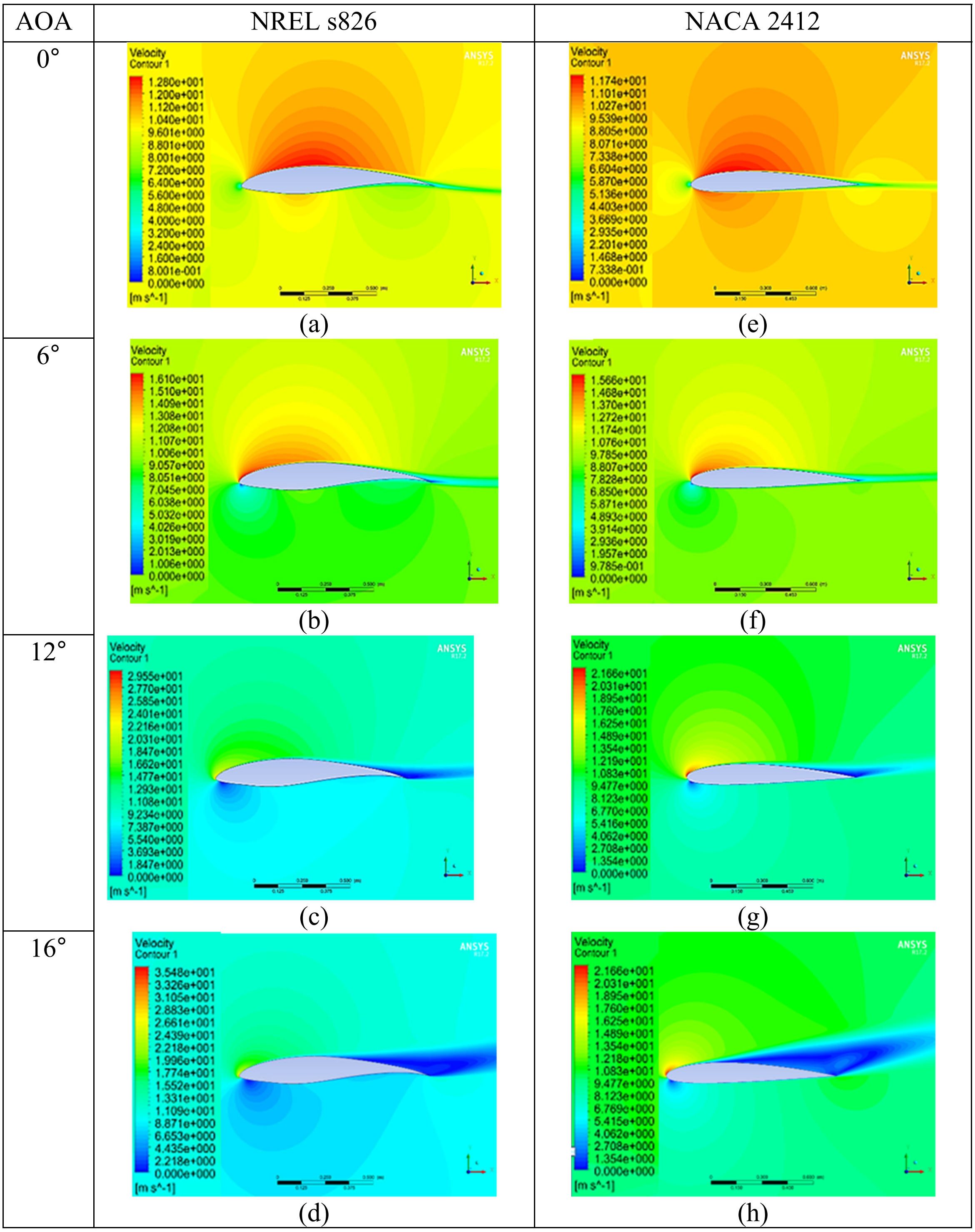

Figure 12: Velocity fields (contours) of airfoils at 9.7 m/s for different AOA.

Pressure Distribution

According to Bernoulli's principle, the increased velocity of airflow over the upper surface of the airfoil creates a lower pressure region, while the slower-moving air beneath results in higher pressure. This contrast in pressure; greater below and lesser above generates the lift force that allows the airfoil to ascend. Thus, the variation in pressure between the upper and lower surfaces of the airfoil, as depicted in Figure 13 (a, b, c, d, e, f, g, h) and Figure 14 (a, b, c, d, e, f, g, h) becomes more pronounced with increasing angle of attack and wind speed. This pressure disparity reaches its peak at angles of 12° and 14° degrees, where the highest lift coefficient values are expected to be achieved. As presented in in Figure 15 (a, b, c, d), the lift coefficient CL has recorded the highest values between angles of attacks 12° and 14° for both types of airfoils at all considered wind speeds (5.5m/s, 7m/s, 8.3m/s, 9.7m/s).

Likewise, the values of Lift force have shown similar trend that recorded for the lift coefficient for all cases as illustrated in Figure 16 (a, b, c, d). These plots show that airfoil s826 provides better higher results than 2412 airfoil at these velocities. This preference can be attributed for that NREL S826 is optimized for delayed stall, meaning it maintains lift better at higher angles of attack before experiencing flow separation. Moreover, The S826 airfoil has a lower drag coefficient, improving aerodynamic efficiency and reducing energy losses.

It can also be noticed that the lift force and coefficients reach their highest value at angles between 12 and 14, and after that they decrease. As the airflow moves around the airfoil, especially over the curved upper surface, it faces an adverse pressure gradient, causing the pressure to rise along the flow direction toward the trailing edge, as illustrated in the Figures 13 and 14. As the airflow circulates around the airfoil, particularly over its curved upper surface, it encounters an adverse pressure gradient, leading to a gradual increase in pressure along the flow direction toward the trailing edge, as shown in the Figures 11 and 12. Significantly, flow separation plays a crucial role in shaping the velocity distribution around the airfoil.

When flow separation takes place, the high-speed airflow over the upper surface is interrupted, causing a significant slowdown in the separated flow. This reduction in speed diminishes the velocity contrast between the upper and lower surfaces, directly affecting lift generation. Since lift depends on the pressure difference between these surfaces, a smaller velocity variation leads to a decreased pressure differential, ultimately resulting in a loss of lift force.

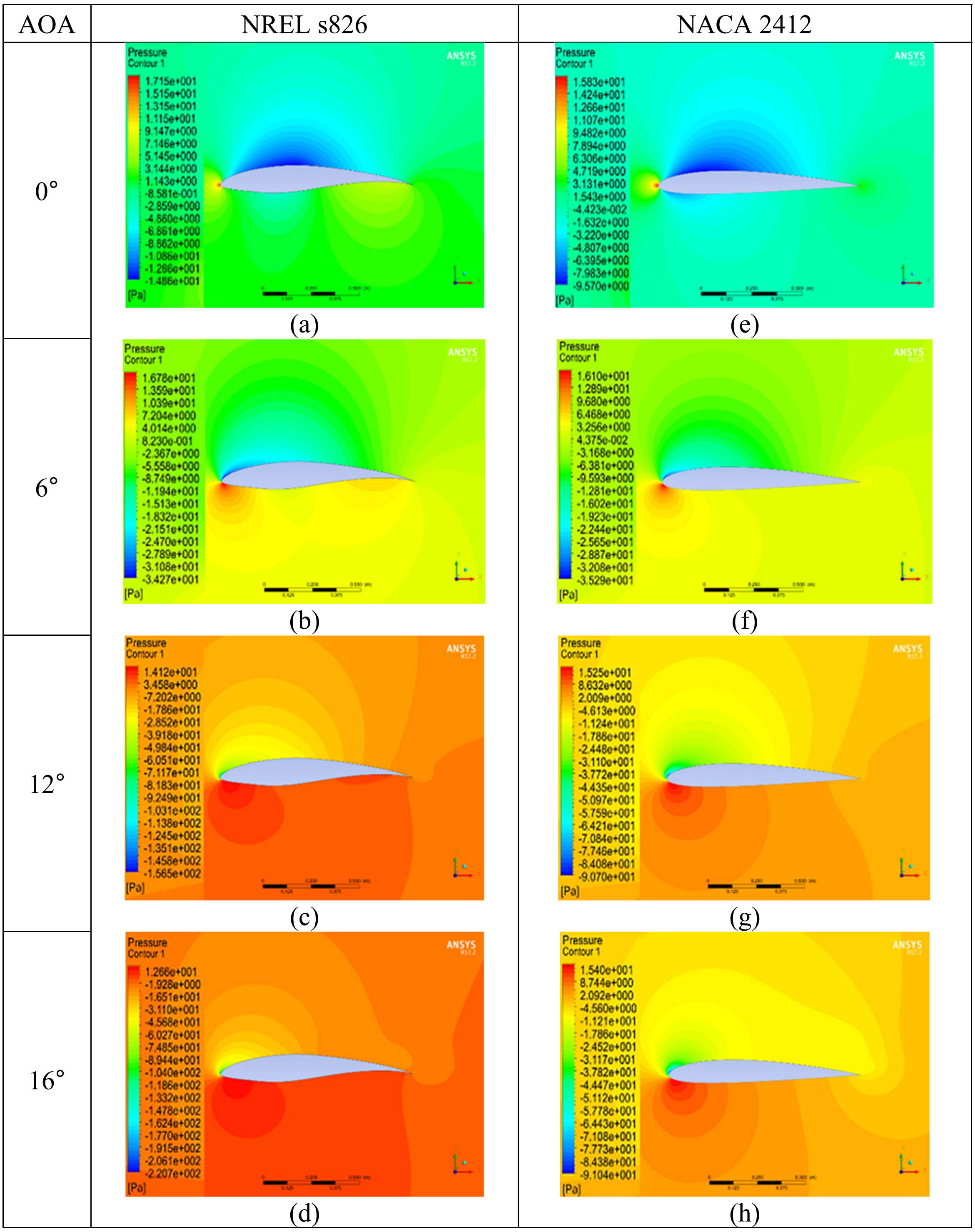

Figure 13: Pressure fields (contours) of airfoils at 5.5 m/s for different AOA.

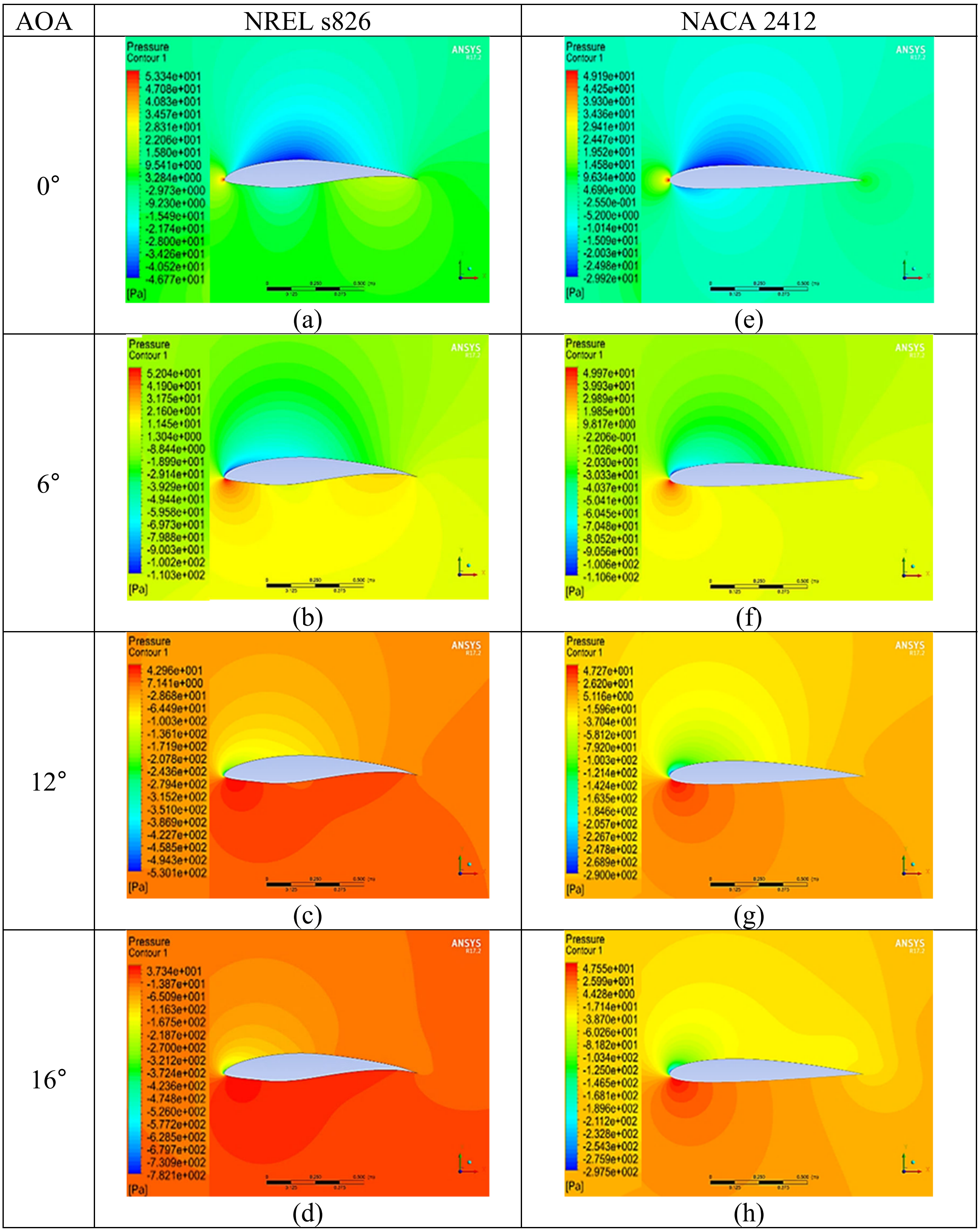

Figure 14: Pressure fields (contours) of airfoils at 9.7 m/s for different AOA.

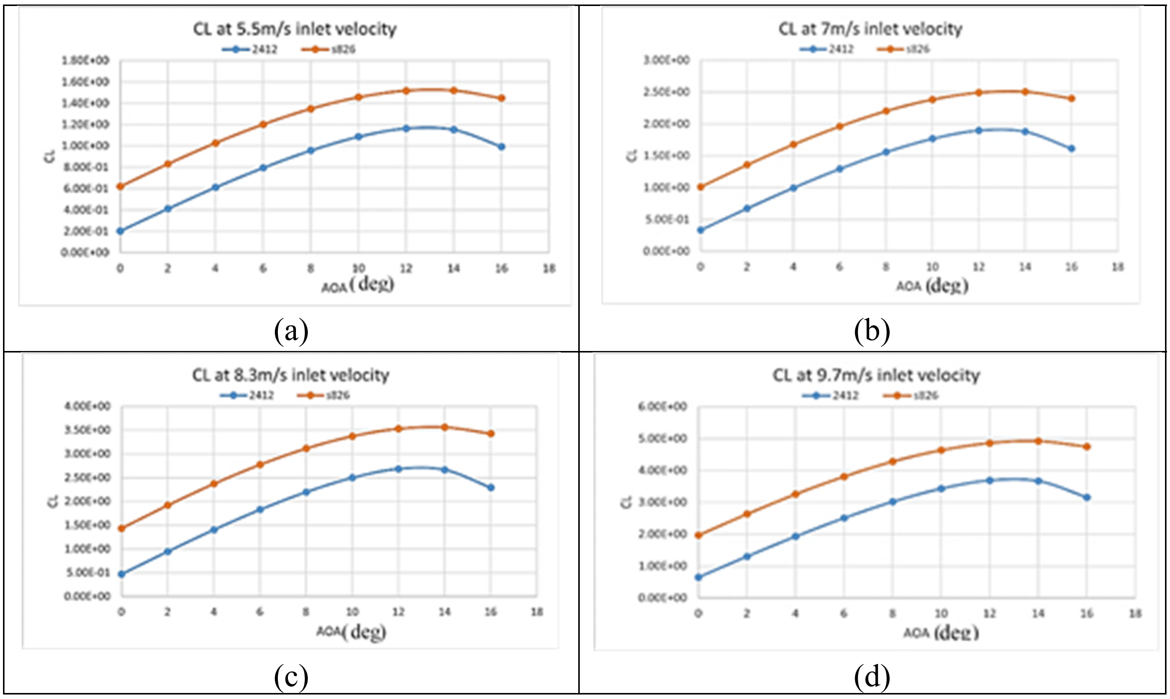

Figure 15: CL against AOA charts at velocities of 5.5m/s, 7m/s, 8.3m/s, and 9.7m/s.

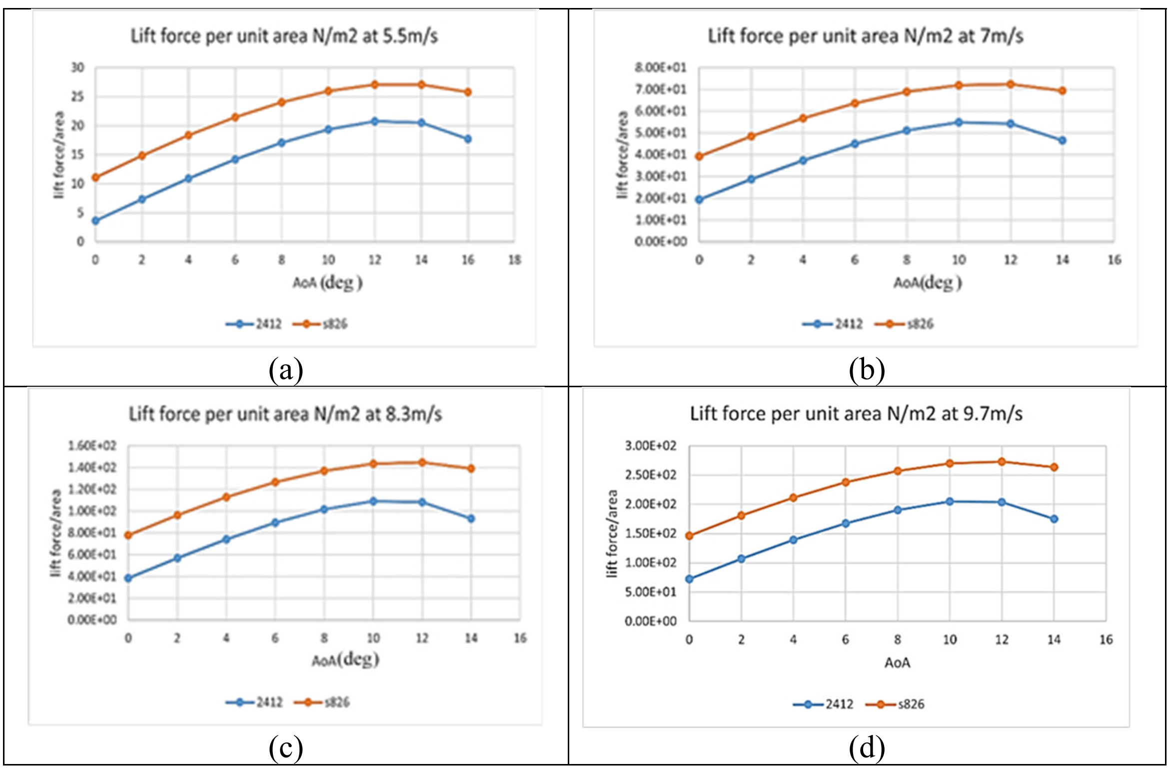

Figure 16: Lift force against AOA charts at velocities of 5.5m/s, 7m/s, 8.3m/s, and 9.7m/s.

CONCLUSION

This study investigated the aerodynamic performance of two airfoils (NREL S826 and NACA 2412) that are used in small scale wind turbines. Two-dimensional numerical models were created for each airfoil, where a computational domain has been created and a mesh was generated. The models were validated using laboratory data to ensure accuracy. These models were then used to simulate the conditions in Yafren town. The pressure and velocity fields around the airfoils were examined, and the lift coefficient and lift force were calculated for different wind speeds and angles of attack. The results were compared to determine which airfoil delivers superior performance for domestic wind turbines in Yefren town, providing a potential alternative energy source.

The current study found that both airfoils exhibit optimal lift performance at angles of attack ranging from 12 to 14 degrees. This is primarily due to the maximum velocity difference between the upper and lower surfaces at these angles, which enhances lift generation. However, at higher angles of attack, lift performance declines significantly due to early flow separation occurring on the airfoil surface. The findings indicate a slight advantage of the NREL S826 airfoil within the optimal angle of attack range of 12 to 14 degrees. This preference is likely attributed to its unique design features, which enhance lift generation under these operating conditions.

LIST OF ABBREVIATIONS

2D	Two dimensional
AOA	Angle of Attack [deg]
Cl	lift coefficient
CLmax	maximum lift coefficient
Cd	drag coefficient
Cp	power factor
CFD	Computational Fluid Dynamics
HAWT	Horizontal Axis Wind Turbine
NREL	National Renewable Energy Laboratory
NACA	National Advisory Committee for Aeronautics
PIV	Particle Image Velocimetry
S-A	Spalart–Allmaras

REFERENCES

[1] Krishnan, S. K., Kandasamy, S., & Subbiah, K, (2021). Fabrication of microbial fuel cells with nanoelectrodes for enhanced bioenergy production, In Nanomaterials, 677-687. Academic Press.

[2] Kılıç, F. Ç. and Öztürk, H. H., (2021). *Energy Management and Energy Efficiency in Industry*, Springer.

[3] Aklin, M. and Urpelainen, J., (2018). Renewables: *The politics of a global energy transition*, MIT Press.

[4] Energy Institute, (2023). Statistical Review of World Energy 2023, in Our world date.

[5] DOE, U.S. Department of Energy, (www.energy.gov).

[6] Letcher, T. M., (2017). Wind Energy Engineering: A Handbook for Onshore and Offshore Wind Turbines, Elsevier Inc.

[7] Caltech Science Exchange, (scienceexchange.caltech.edu/).
[8] Global wind energy council, (www.gwec.net).
[9] IEA Wind TCP, (iea-wind.org).
[10] International Renewable Energy Agency, IRENA, (www.irena.org/Energy-Transition/Technology/Wind-energy).
[11] Ishfaq, S. M., and Chaudhry, H. N., (2018). Numerical investigation of the optimum wind turbine sitting for domestic flat roofs, *Sustainable Buildings*, 3(2).
[12] Rhodes, J. S., (2014). Understanding Wind Power Technology, John Wiley & Sons Ltd.
[13] Wind energy, (2018). Journal Metrics: *Wind Energy*, John Wiley & Sons Ltd.
[14] Perera, S. M., Putrus, G., Conlon, M., Narayana, M., and Sunderland, K., (2022). Wind energy harvesting and conversion systems: A technical review, *Energies*, 15(24), 9299.
[15] Nakhchi, M. E., Naung, S. W., and Rahmati, M., (2021). High-resolution direct numerical simulations of flow structure and aerodynamic performance of wind turbine airfoil at wide range of Reynolds numbers, *Energy*, 225, 120261.
[16] Salem, A., Hamza, E., Nassar Y. and Hmmady, I., (2023). Numerical Simulation of Aerodynamics Performance of NERL S826 Airfoil, 8th International Engineering Conference on Renewable Energy & Sustainability, ieCRES, Gaza, State of Palestine, 1-6, doi: 10.1109/ieCRES57315.2023.10209478.
[17] Kanyako, F., and Janajreh, I., (2014). Numerical investigation of four commonly used airfoils for vertical axis wind turbine, In ICREGA 14-Renewable Energy: Generation and Applications, 443-454, Springer International Publishing.
[18] Hamza, E., (2016). A review of using computational fluid dynamic in simulating of friction stir welding and parametric studies, 11th International Symposium on FSW, Cambridge, UK.
[19] Matsson, J. E., Voth, J. A., McCain, C. A., & McGraw, C., (2016). Aerodynamic performance of the NACA 2412 airfoil at low Reynolds number, In 2016 ASEE Annual Conference & Exposition.
[20] Kandwal, S. and Singh, S., (2012). Computational Fluid Dynamics Study Of Fluid Flow And Aerodynamic Forces on an Airfoil, *International Journal of Engineering Research & Technology (IJERT)*, 1(7).
[21] Singh, R. K., Ahmed, M. R., Zullah, M. A., and Lee, Y. H., (2012). Design of a low Reynolds number airfoil for small horizontal axis wind turbines, *Renewable energy*, 42, 66-76.
[22] Ali, A., Chowdhury, H., Loganathan, B., and Alam, F., (2015). An aerodynamic study of a domestic scale horizontal axis wind turbine with varied tip configurations, *Procedia Engineering*, 105, 757-762.
[23] Van, T. D., Huu, D. N., and Le Quang, S., (2024). Consideration of various configurations of SG6043-based rotor applied in small capacity horizontal axis wind turbine, *International Journal of Renewable Energy Development*, 13(3), 396-404.
[24] Görgülü, Y. F., Özgür, M. A., and Köse, R., (2021). CFD analysis of a NACA 0009 aerofoil at a low reynolds number, *Politeknik Dergisi*, 24(3), 1237-1242.
[25] Islam, M., Fürst, J., and Wood, D., (2017). CFD Analysis of SD 7003 Airfoil at Low Reynolds Number with a Laminar Kinetic Energy Based Transition Model, *ARPN Journal of Engineering and Applied Sciences*, 12(10).

[26] Mollica, E., and Timmoneri, A., (2021). CFD analysis of the low Reynolds S1223 airfoil, *International Journal of Engineering Science and Technology*, 13(4), 46-49.
[27] Airfoil tools, (airfoiltools.com/airfoil/details?airfoil=s826-nr).
[28] ANSYS, (www.ansys.com/news-center/press-releases/05-%2009-16-ansys-171-delivers-optimized-system-performance-for-early-design-process).
[29] Samuel, M. S. G. and Rajendran, P., (2019). CFD validation of NACA 2412 airfoil, Technical Report, Universiti Sains Malaysia.
[30] Krogstad, P. Å., and Eriksen, P. E., (2013). Blind Test Calculations of the Performance and Wake Development for a Model Wind Turbine, *Renewable energy*, 50, 325-333.
[31] Hamza, E., Asim, T., and Mishra, R., (2016). Computational Fluid Dynamics based Transient Thermal Analysis of Friction Stir Welding, In proceedings of the 6th International and 43rd National Conference on Fluid Mechanics and Fluid Power, Allahabad, India.
[32] Hamza, E., (2020). Dimensions Effect of the Rotating Fluid Zone on the Results when CFD Modeling of Friction Stir Welding, In the International Conference for Engineering Sciences and Technology (CEST-2020), 3, AL-Khoms/ Libya.
[33] Hamza, E. (2021). CFD-modelling and Thermal Characterization of Friction Stir Welding using Tool with Polygonal Pins, *Journal of Engineering Research*, 32, 43-78.